代表作

The PVDF-based wave number domain sensing techniques for active sound radiation control from a simply supported beam

Bor-Tsuen Wang

Department of Mechanical Engineering, National Pingtung University of Science and Technology, Pingtung, Taiwan 91207, Republic of China

(Received 22 August 1996; accepted for publication 10 December 1997)

This work presents a novel wave number domain sensing approach which applies polyvinylidene fluoride (PVDF) films for active structural acoustic control. An array of PVDF strip films is equally distributed over a beam to measure the structural response. The PVDF voltage wave number transform functions can then be obtained by performing the discrete wave number transform on the sensing signals. The cost function can be defined as the sum of mean square values of the supersonic components of the wave number transform function. The linear quadratic optimization process can be applied to obtain the optimal control inputs, thereby minimizing the cost function. This work also considers the simply supported beam with infinite rigid baffle subjected to a harmonic point force disturbance. The PVDF-based wave number domain sensing approach is applied, while piezoelectric actuators are used as control inputs. In addition, the sensing method's performance is evaluated by comparing with an accelerometer based wave number domain sensing approach. Both continuous and discrete wave number transform approaches are presented as well. Analysis results demonstrate that the wave number domain sensing approach cannot only provide efficient signals that are related to the structure-borne sound, but is also quite effective in controlling sound radiation. This work advances current efforts to apply the sensing ability of intelligent material structure systems to actively control structural sound radiation. © *1998 Acoustical Society of America.* [S0001-4966(98)05103-0]

PACS numbers: 43.40.Vn [PJR]

LIST OF SYMBOLS

$\tilde{A}$	acceleration wave number transform function derived from the CWT approach
$\tilde{A}_{\mathrm{DWT}}$	acceleration wave number transform function derived from the DWT approach
A	PVDF film area
b	beam width
b_p	PVDF width
c	phase speed of sound in air
E_b	beam Young's modulus
e_{31}	piezoelectric strain constant of PVDF sensor
F	point force magnitude
$g_n(r,\theta,\phi)$	the nth pressure modal amplitude
$H_n(\omega)$	the nth mode transfer function
i	spatial sequence for the DWT approach
I	moment of inertia of the beam
K_p	some constant related to PVDF material properties
L	beam length
l_c	length of PZT actuator
l_p	length of PVDF sensor
M_{eq}	equivalent moment induced by PZT actuator
m	wave number sequence for the DWT approach
N	number of spatial samples or number of sensors
N_κ	minimum number of wave number sequence such that $\min(N_k)>(\kappa/\Delta\kappa_x)+1$
p_c, p_f, p_t	sound pressure due to PZT actuator, point force disturbance and total
$q_n(\omega)$	the nth modal amplitude
$q_n^c(\omega)$	the nth modal amplitude due to PZT actuators
$q_n^f(\omega)$	the nth modal amplitude due to point force (disturbance)
r,θ,ϕ	radiation field coordinates
t_b	beam thickness
t_p	PVDF thickness
$V(x,t)$	generated voltage from PVDF sensor
$\tilde{V}$	PVDF voltage wave number transform function derived from the CWT approach
$\tilde{V}_{\mathrm{DWT}}$	PVDF voltage wave number transform function derived from the DWT approach
$w(x,t)$	beam lateral displacement
x_a	accelerometer location (Fig. 1)
x_c, x_1, x_2	PZT actuator location (Fig. 1)
x_f	force location (Fig. 1)
x_p, x_{p1}, x_{p2}	PVDF sensor location (Fig. 1)
α_n	normal mode wave number
Δx	spacing between sensors
$\Delta\kappa_x$	wave number resolution
$\delta(x)$	Kronecker delta function
ϵ	permittivity of PVDF film
$\Gamma(x)$	shape function of the PVDF sensor
κ	acoustic wave number
κ_x, κ_y	structural wave number
$\kappa_{x,\mathrm{Nyq}}$	Nyquist wave number
$\omega = 2\pi f$	excitation frequency
ω_n	the nth natural frequency
Φ_p	radiated sound power

 0001-4966/98/103(4)/1904/12/$10.00

$\Phi_{\kappa,\tilde{V}}$	cost function for PVDF-based wave number sensing by the CWT approach
$\Phi_{\kappa,\tilde{A}}$	cost function for accelerometer based wave number sensing by the CWT approach
$\Phi_{\kappa,\tilde{V}_{\mathrm{DWT}}}$	cost function for PVDF-based wave number sensing by the DWT approach
$\Phi_{\kappa,\tilde{A}_{\mathrm{DWT}}}$	cost function for accelerometer based wave number sensing by the DWT approach
$\phi_n(x)$	the nth displacement mode shape of the simply supported beam
$\phi_n^c(x)$	the nth PZT actuator mode shape of the simply supported beam
$\phi_n^f(x)$	the nth point force mode shape of the simply supported beam
$\phi_n^p(x)$	the nth PVDF sensor mode shape of the simply supported beam
$\tilde{\phi}_n(\kappa_x)$	wave number transform of $\phi_n(x)$
$\tilde{\phi}_n^p(\kappa_x)$	wave number transform of $\phi_n^p(x)$
ρ	air density
ρ_b	beam density

INTRODUCTION

Structural-borne sound radiation control has received extensive interest, particularly in terms of developing actuators,[1-4] sensors,[5-7] and control algorithms.[8-10] This work presents a novel PVDF based wave number domain sensing technique.

Microphones are conventional error sensors used for active noise control.[11,12] However, such a far-field sensor cannot be implemented for certain applications. In attempting to resolve this problem, some researchers have used the structural sensors such as accelerometers[6] instead of acoustic sensors. Although sufficient control can be achieved, using many accelerometers not only increases the cost, but also influences the original structure's physical characteristics. The feasibility of using polyvinylidene fluoride (PVDF) sensors for structural sound or vibration control has received increasing interest.[13-15] Either a strip of PVDF film[14,15] or a preshaped PVDF modal sensor[13] can be effectively applied to active structural sound radiation control.[13-15] The performance of accelerometers, microphones, and PVDF strip sensors in active structural acoustic control has been studied.[16-18] Microphones generally perform better sound radiation control than the other two; however, microphones have some drawbacks as mentioned above. Among the merits of PVDF sensors include its lower cost, thinner film, and easier implementation than accelerometers. Most importantly, the PVDF films do not induce a mass effect on structures such as accelerometers. Various types of design of PVDF film sensors have been proposed[19-23] and quite promising for controlling structural sound radiation.

As generally known, structural sound radiation can be determined by wave number domain analysis.[24] Only structural wave number components less than the acoustic wave number radiate sound into the far field and, therefore, are termed as supersonic waves. In contrast, the subsonic waves do not contribute to sound radiation. According to previous investigations, wave number domain analysis is a highly effective means of examining the mechanism of structural sound radiation control.[18,25] Such analysis also induces the notion of a wave number domain approach to actively control structure-borne sound. Fuller and Burdisso[26] formulated a cost function on the basis of the wave number domain components associated with the angle of sound radiation to be controlled. The sound radiation can subsequently be effectively controlled. Clark and Fuller[27] analytically demonstrated the model reference control approach while considering the wave number transform of accelerations, corresponding to the desired far field acoustic directivity pattern. According to their results, the wave number distributions can be largely reduced in the supersonic region, thereby allowing for efficiently controlling sound radiation. Maillard and Fuller[28,29] employed accelerometers as error sensors to construct the cost function, i.e., the wave number component associated with a prescribed radiation angle based on the discrete wave number transform. Scott and Sommerfeldt[30] recently investigated the use of an array of shaped PVDF sensors to act as low-pass filters to estimate the radiated power of clamped beams. They showed that the distributed shaped sensors can provide better predictions than the point sensors.

In light of the promising nature of PVDF sensors and wave number domain sensing approaches, this work presents a novel wave number domain sensing technique, in which an array of PVDF strip films attached to the beam is applied. The PVDF sensors are evenly spaced over the beam. The structural response can then be measured and taken by discrete wave number transform to derive the wave number transform function of the PVDF voltage. The cost function, defined as the sum of mean square values of the supersonic wave number components of the wave number transform functions, is related to the radiated power. The linear quadratic optimal control theory can then be applied to determine the control input, thereby minimizing the cost function. Analysis results demonstrates that the sensing technique, in conjunction with the LMS feedforward control algorithm, efficiently reduces the sound radiation from the beam into the far field.

I. THEORETICAL ANALYSIS

A. Lateral vibration of uniform beam

Consider a uniform simply supported beam with length L, as depicted in Fig. 1. The beam lateral displacement, due to harmonic excitation, can be expressed as follows:

$$w(x,t) = e^{j\omega t} \sum_{n=1}^{\infty} q_n(\omega)\,\phi_n(x), \tag{1}$$

where

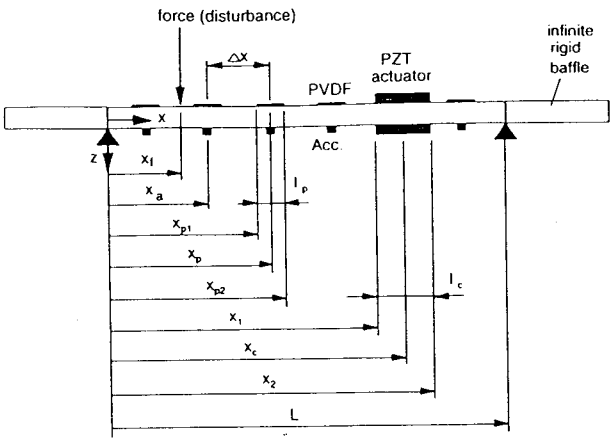

FIG. 1. The arrangement and coordinates of simply supported beam.

$$\phi_n(x) = \sin\ \alpha_n x, \tag{2}$$

$$\alpha_n = \frac{n\pi}{L}. \tag{3}$$

The modal amplitudes $q_n(\omega)$ rely on the form of the excitation force. For a harmonic point force F applying at x_f, the modal amplitude can be shown as

$$q_n^f(\omega) = H_n(\omega)\phi_n^f(x_f)F, \tag{4}$$

where

$$H_n(\omega) = \frac{1}{\rho_b b t_b(\omega_n^2 - \omega^2)}, \tag{5}$$

$$\omega_n = \alpha_n^2 \sqrt{\frac{E_b I}{\rho_b b t_b}}, \tag{6}$$

$$\phi_n^f(x_f) = \sin\ \alpha_n x_f. \tag{7}$$

Notably, $\phi_n^f(x_f)$ denotes the displacement mode shape of the beam at coordinate x_f. For an actuator consisting of two identical piezoceramic patches, bonded symmetrically on the two opposite beam surfaces, and activated 180° out-of-phase, the corresponding modal amplitude can be derived as follows:

$$q_n^c(\omega) = H_n(\omega)\phi_n^c(x_f)M_{\text{eq}}, \tag{8}$$

where

$$\phi_n^c(x_c) = \phi_n'(x_1) - \phi_n'(x_2) = 2\alpha_n\ \sin(\alpha_n l_c/2)\phi_n(x_c). \tag{9}$$

Notably, $\phi_n^c(x_c)$ is the PZT actuator mode shape and represents the slope difference between the two edges of the PZT actuator at coordinates x_1, x_2. Also, $\phi_n^c(x_c)$ can be expressed as the displacement mode shape of the beam at the central location of the PZT patch, x_c, for the simply supported beam. For a PVDF film arranged as Fig. 1 illustrates, the generated voltage can be written as[14]

$$V(x_p, t) = e^{j\omega t}K_p\sum_{n=1}^{\infty} q_n(\omega)\phi_n^p(x_p), \tag{10}$$

where

$$\phi_n^p(x_p) = \phi_n'(x_{p1}) - \phi_n'(x_{p2}) = 2\alpha_n\ \sin(\alpha_n l_p/2)\phi_n(x_p), \tag{11}$$

$$K_p = \frac{t_p}{\epsilon A}\frac{t_b + t_p}{2} e_{31} b_p. \tag{12}$$

Notably, the generated voltage is proportional to the slope difference between the two edges of the PVDF film. In addition, Eq. (11) indicates that the PVDF sensor mode shape $\phi_n^p(x_p)$ is related to the displacement mode shape at the central location of the PVDF sensor and weighted by the factor $2\alpha_n\ \sin(\alpha_n l_p/2)$.

B. Sound radiation from the beam

The far-field radiated sound pressure from the beam with infinite rigid baffle due to the point force and PZT actuator can be derived from the Rayleigh integral, respectively,

$$p_f(r,\theta,\phi,t) = e^{j\omega t}\sum_{n=1}^{\infty} H_n(\omega)\phi_n^f(x_f)Fg_n(r,\theta,\phi), \tag{13}$$

$$p_c(r,\theta,\phi,t) = e^{j\omega t}\sum_{n=1}^{\infty} H_n(\omega)\phi_n^c(x_c)M_{eq}g_n(r,\theta,\phi), \tag{14}$$

where

$$g_n(r,\theta,\phi) = -j\omega\frac{\rho c b}{\pi}\frac{\kappa}{\alpha_n}\frac{e^{-j\kappa r}}{2r}\left[\frac{1-(-1)^n e^{-j\alpha}}{1+(\alpha/n\pi)^2}\right] \times\left[\frac{1-e^{-j\beta}}{\beta}\right], \tag{15}$$

$$\alpha = \kappa L\ \sin\ \theta\ \cos\ \phi, \tag{16}$$

$$\beta = \kappa b\ \sin\ \theta\ \sin\ \phi. \tag{17}$$

Under the assumption of superposition, the total radiated sound pressure denotes the sum of the sound pressures attributed to the disturbance and control inputs

$$p_t = p_f + p_c = e^{j\omega t}\sum_{n=1}^{\infty}[\phi_n^f(x_f)F + \phi_n^c(x_c)M_{eq}]H_n(\omega)g_n(r,\theta,\phi). \tag{18}$$

The total radiated power, defined as the integral of the square of the radiated sound pressure over the hemisphere of the radiating field, can then be obtained as

$$\Phi_p = \frac{1}{2\rho c}\int_s |p_t|^2 dS = \frac{r^2}{2\rho c}\int_0^{2\pi}\int_0^{\pi/2}|p_t|^2\ \sin\ \theta\, d\theta\, d\phi. \tag{19}$$

The total radiated sound power can be an index to evaluate the effectiveness of controlling the sound radiation.

C. Wave number analysis

By performing continuous wave number transform (CWT) in terms of spatial coordinates for a two-dimensional

rectangular radiator, the acceleration wave number transform function can be obtained by neglecting the harmonic time function, i.e.,

$$\tilde{A}(\kappa_x,\kappa_y)=\int_{-\infty}^{\infty}\int_{-\infty}^{\infty}\ddot{w}(x,y)e^{-j(\kappa_x x+\kappa_y y)}\,dx\,dy, \quad (20)$$

where

$$\kappa_x=\kappa\sin\theta\cos\phi, \quad (21)$$

$$\kappa_y=\kappa\sin\theta\sin\phi. \quad (22)$$

For a one-dimensional beam application, the y-direction response is negligible. Therefore, the beam acceleration wave number transform function (WTF), by performing the continuous wave number transform and neglecting the time component, can be expressed as

$$\tilde{A}(\kappa_x,\kappa_y)=-\omega^2\left[\frac{e^{-j\kappa_y b}-1}{-j\kappa_y}\right]\sum_{n=1}^{\infty}q_n(\omega)\tilde{\phi}_n(\kappa_x), \quad (23)$$

where

$$\tilde{\phi}_n(\kappa_x)=\int_{-\infty}^{\infty}\phi_n(x)e^{-j\kappa_x x}\,dx$$

$$=\int_0^L\phi_n(x)e^{-j\kappa_x x}\,dx=\alpha_n\left[\frac{1-(-1)^n e^{-j\kappa_x L}}{\alpha_n^2-\kappa_x^2}\right]. \quad (24)$$

$\tilde{\phi}_n(\kappa_x)$ is the continuous wave number transform of $\phi_n(x)$, and can be approximated by the discrete wave number transform (DWT) as follows:

$$\tilde{\phi}(m\Delta\kappa_x)=\sum_{i=1}^{N}\phi_n(i\Delta x)e^{-j(mi/N)}\Delta x,$$

$$m=-(N-1),-(N-2),\ldots,-1,0,1,\ldots,N-1, \quad (25)$$

where

$$\Delta\kappa_x=\frac{1}{L}, \quad (26)$$

$$N=\frac{L}{\Delta x}. \quad (27)$$

N denotes the number of discretization, i.e., the number of sensors applied in practical measurement; and Δx represent the equal distance between accelerometers. The acceleration WTF by performing the DWT for $\kappa_y=0$, i.e., only the κ_x components are considered in this work, can then be derived as

$$\tilde{A}_{\mathrm{DWT}}(m\Delta\kappa_x)=-b\omega^2\sum_{n=1}^{\infty}q_n(\omega)\tilde{\phi}_n(m\Delta\kappa_x)$$

$$m=-(N-1),-(N-2),\ldots,-1,0,1,\ldots,N-2,N-1. \quad (28)$$

Notably, the negative wave number components (m=negative integer) are also included and simply correspond to radiation in opposite directions from the positive wave number ones.

Similarly, the generated voltages from the PVDF film shown in Eq. (10) can also be taken by the CWT in κ-plane and derived as follows:

$$\tilde{V}(\kappa_x,\kappa_y)=K_p\left[\frac{e^{-j\kappa_y b}-1}{-j\kappa_y}\right]\sum_{n=1}^{\infty}q_n(\omega)\tilde{\phi}_n^p(\kappa_x), \quad (29)$$

where

$$\tilde{\phi}_n^p(\kappa_x)=\int_0^L\phi_n^p(x)e^{-j\kappa_x x}\,dx$$

$$=2\alpha_n^2\sin(\alpha_n l_p/2)\left[\frac{1-(-1)^n e^{-j\kappa_x L}}{\alpha_n^2-\kappa_x^2}\right]. \quad (30)$$

Again, the continuous wave number transform of the PVDF voltage shown in Eq. (29) can be approximated by the discrete wave number transform; therefore, the PVDF voltage WTF by performing the DWT for $\kappa_y=0$ can be obtained as

$$\tilde{V}_{\mathrm{DWT}}(m\Delta\kappa_x)=-b\sum_{n=1}^{\infty}q_n(\omega)\tilde{\phi}_n^p(m\Delta\kappa_x),$$

$$m=-(N-1),-(N-2),\ldots,-1,0,1,\ldots,N-2,N-1, \quad (31)$$

where

$$\tilde{\phi}_n^p(m\Delta\kappa_x)=\sum_{i=1}^{N}\phi_n^p(i\Delta x)e^{-j(mi/N)}\Delta x,$$

$$m=-(N-1),-(N-2),\ldots,-1,0,1,\ldots,N-2,N-1. \quad (32)$$

$\tilde{\phi}_n^p(m\Delta\kappa_x)$ denotes the mth wave number components of the PVDF mode shape $\phi_n^p(x)$ by performing the discrete wave number transform; and $i\Delta x$ represents the spatial coordinate of the ith sensor location.

D. Cost functions

Notably, the mean-square value of the acceleration wave number transform function, i.e., $|\tilde{A}|^2$, integrated over the supersonic region is related to the radiated power.[24] Only the wavenumber components satisfying $\kappa_x^2+\kappa_y^2<\kappa^2$ contribute to sound radiation into the far field, and are termed herein as the supersonic waves. The other wave number components associated with subsonic waves do not radiate into the far field. For a one-dimensional beam with infinite rigid baffle, the radiated power can be expressed in terms of the wave number transform of beam acceleration as follows:[31]

$$\Phi_p=\frac{\rho c\kappa}{4\pi\omega^2}\int_{-\kappa}^{\kappa}\frac{|\tilde{A}(\kappa_x)|^2}{\sqrt{\kappa^2-\kappa_x^2}}\,d\kappa_x. \quad (33)$$

Precisely evaluate the above integral is extremely difficult. Cremer and Heck[31] proposed an approximate method to estimate the radiated power. Herein, the cost function can be constructed on the basis of the wave number transform functions introduced in Eqs. (23) and (29). Two types of cost

functions associated with the wave number components in supersonic region are defined as follows:

$$\Phi_{\kappa,\tilde{A}} = \int_{-\kappa}^{\kappa} |\tilde{A}(\kappa_x, \kappa_y = 0)|^2 \, d\kappa_x, \tag{34}$$

$$\Phi_{\kappa,\tilde{V}} = \int_{-\kappa}^{\kappa} |\tilde{V}(\kappa_x, \kappa_y = 0)|^2 \, d\kappa_x, \tag{35}$$

where $\Phi_{\kappa,\tilde{A}}$ denotes the integration of supersonic wave number components that contribute to the sound radiation into the far field, and is strongly related to the radiated power. Also, $\Phi_{\kappa,\tilde{V}}$ represents the integration of the mean square value of PVDF voltage wave number transform functions over the supersonic region. Closely examining Eqs. (23) and (29) reveals two main differences. First, constants $-\omega^2$ and K_p [defined in Eq. (12)] are premultiplied for $\tilde{A}$ and $\tilde{V}$, respectively. Second, $\tilde{\phi}_n(\kappa_x)$ and $\tilde{\phi}_n^p(\kappa_x)$ represent $\tilde{A}$ and $\tilde{V}$ in the summation respectively. $\tilde{\phi}_n(\kappa_x)$ and $\tilde{\phi}_n^p(\kappa_x)$ are obtained by performing the wave number transform on $\phi_n(x)$ and $\phi_n^p(x)$. Notably, $\phi_n^p(x)$ as defined in Eq. (11) is the slope difference between the two edges of the PVDF film.[32,33] In particular, $\phi_n^p(x)$ is related to the displacement mode shape $\phi_n(x)$ for the case of a simply supported beam. Comparing Eqs. (24) and (30) indicates that $\tilde{\phi}_n(\kappa_x)$ and $\tilde{\phi}_n^p(\kappa_x)$ have the same form of functions in terms of κ_x. Therefore, cost functions $\Phi_{\tilde{A}}$ and $\Phi_{\tilde{V}}$ can be strongly correlated and also related to the radiated power for the simply supported beam, as shown in Eq. (33). Both $\Phi_{\kappa,\tilde{A}}$ and $\Phi_{\kappa,\tilde{V}}$ are continuous functions obtained from the acceleration and PVDF voltage wave number transform functions, based on the CWT approach. Importantly, these two cost functions can not be directly measured in practice, despite the fact that these cost functions are highly correlated with the structural sound radiation.

Employing an array of evenly spaced accelerometers or PVDF strip film sensors in conjunction with the DWT approach allows us to derive the discrete wave number transform functions based on accelerometers and PVDF sensors through Eqs. (23) and (29), as shown in Eqs. (28) and (31). Both negative and positive wave number components can subsequently be obtained. Moreover, the symmetry of $|\tilde{V}(\kappa_x)|^2$ and $|\tilde{A}(\kappa_x)|^2$ and the folding effect of discrete wave number transform (analogous to the time domain Fourier transform), enable us to also obtain negative wave number components without the discrete wave number transform on the negative integer m. Notably, only the wave number components below and above the Nyquist wave number $\pm \kappa_{x,\mathrm{Nyq}} = (N/2)\Delta\kappa_x$ are valid. Analogous to Eqs. (34) and (35) for the CWT approach, the cost functions based on the DWT approach for accelerometers and PVDF sensors can be defined as

$$\Phi_{\kappa,\tilde{A}_{\mathrm{DWT}}} = \sum_{m=-N_k}^{N_k} |\tilde{A}_{\mathrm{DWT}}(m\Delta\kappa_x)|^2,$$

$$\min(N_k) > \frac{\kappa}{\Delta\kappa_x} + 1, \tag{36}$$

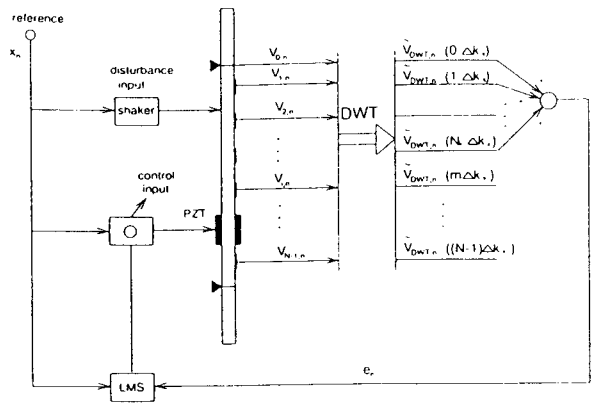

FIG. 2. LMS model for PVDF-based wave number sensing approach.

$$\Phi_{\kappa,\tilde{V}_{\mathrm{DWT}}} = \sum_{m=-N_k}^{N_k} |\tilde{V}_{\mathrm{DWT}}(m\Delta\kappa_x)|^2,$$

$$\min(N_k) > \frac{\kappa}{\Delta\kappa_x} + 1. \tag{37}$$

$\Phi_{\kappa,\tilde{A}_{\mathrm{DWT}}}$ and $\Phi_{\kappa,\tilde{V}_{\mathrm{DWT}}}$ represent the sum of mean square values of the supersonic wave number components of the acceleration and PVDF voltage WTFs, respectively. In addition, N_k denotes the minimum number of wave number components such that $\min(N_k) > (\kappa/\Delta\kappa_x) + 1$. Interestingly, $\Phi_{\kappa,\tilde{A}_{\mathrm{DWT}}}$ and $\Phi_{\kappa,\tilde{V}_{\mathrm{DWT}}}$ are measurable, and can be used to approximate the cost functions $\Phi_{\kappa,\tilde{A}}$ and $\Phi_{\kappa,\tilde{V}}$. In summary, $\Phi_{\kappa,\tilde{A}}$ and $\Phi_{\kappa,\tilde{V}}$ derived from the CWT approach are ideal cost functions, which are not measurable. $\Phi_{\kappa,\tilde{A}_{\mathrm{DWT}}}$ and $\Phi_{\kappa,\tilde{V}_{\mathrm{DWT}}}$ are defined from the acceleration and PVDF voltage WTFs by the DWT approach, and can be obtained by using an array of equally spaced accelerometers and PVDF sensors, respectively. Figure 2 depicts the control block diagram for the PVDF based wave number sensing approach, in conjunction with the use of LMS feedforward control algorithm. Maillard and Fuller provide further detail regarding the implementation.[28,29]

Any of the abovementioned cost functions is obviously quadratic and positively definite; such a function possesses a unique minimum as well. The linear quadratic optimal control theory (LQOCT) can then be applied to minimize the cost function, thereby allowing us derive the optimal control voltages input to the piezoelectric actuators. Minimization procedures[12] can easily calculate the optimal control parameters, subsequently minimizing the cost function. A complete analysis can be referred to[34] and, therefore, is omitted here.

II. NUMERICAL RESULTS AND DISCUSSIONS

A steel beam having dimensions of a length of 0.38 m, width of 0.04 m, and thickness of 2 mm is used in the simulations. The first few natural frequencies are 33.2, 128.8, 289.9, 515.4, 805.3, and 1159.6 Hz. Notably, no damping occurs in the following analysis. Although the optimal process can adequately control multiple primary sources, only one harmonic point force with input parameters, $F = 0.3N$ and $x_f = 0.067$ m, is considered in the following analysis.

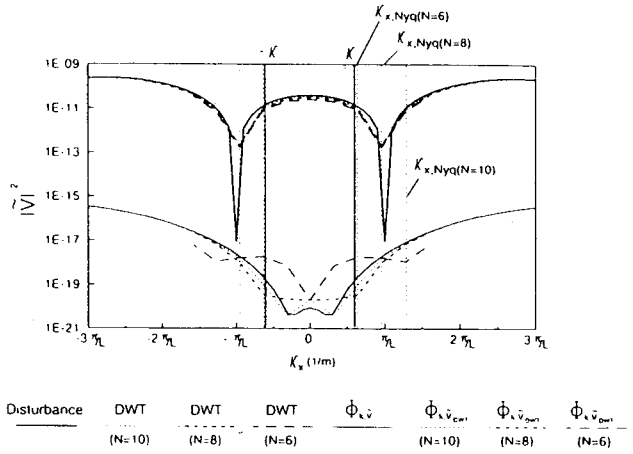

FIG. 3. PVDF voltage wave number spectra before and after being controlled for PVDF sensors, $f=290$ Hz.

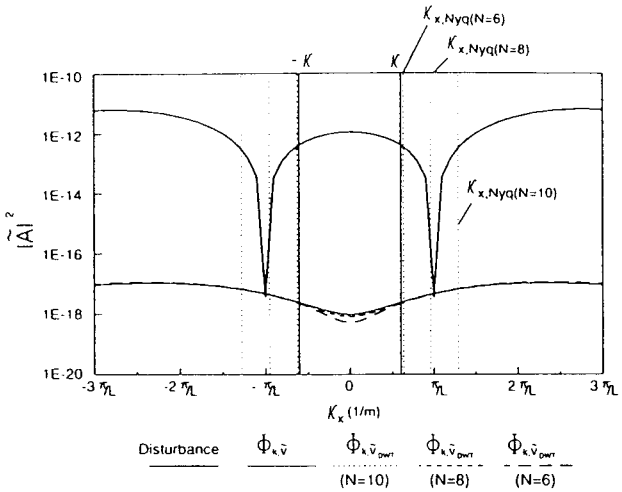

FIG. 4. Acceleration wave number spectra before and after being controlled for PVDF sensors, $f=290$ Hz.

The piezoceramic patch (G-1195)[35] and PVDF films (LDT-28 μm)[36] are used, respectively. The piezoceramic patch is located at $x_1=0.285$ m, $x_2=0.3485$ m. To implement the wave number sensing approach, an array of PVDF strip films are evenly distributed over the beam, length as shown in Fig. 1. Notably, the rectangular shapes of PVDF films, rather than other shapes of PVDF films,[15,21,30] are adopted herein to implement the wave number sensing approach. The PVDF strip film is assumed to be 0.02 m in length for wave number sensing approaches.

For comparison, an array of accelerometers are also used and assumed to be located at the PVDF films' central location, thereby allowing us to implement the wave number sensing approach. Next, the controllability of the wave number sensing approaches is examined, by numerically simulating the cost function derived from the CWT approach in Eqs. (34) and (35). According to those equations, on- and off-resonance excitation cases demonstrate the effectiveness of controlling sound radiation. Either accelerometers or PVDF sensors are respectively used; the CWT and DWT approaches are compared as well. Simulation results of the radiation directivity and WTF distributions demonstrate the control mechanisms of the wave number sensing approaches. The radiated sound pressure is calculated at a radial distance of 3 m from the beam, and plotted in dB *re:* 20×10^{-6} Pa over $\theta=-90°$ to 90° for $\phi=0°$. To calculate the beam response and radiated sound pressure, the modal sums in Eq. (1) must be truncated. While considering computational time and accuracy, the first ten modes are considered and can provide sufficient convergence of the series. Finally, the cases involving different excitation frequencies up to 1000 Hz are also simulated. The cost functions and the radiated powers are plotted against the excitation frequency for both before and after being controlled, respectively.

A. On-resonance excitation case, $f=290$ Hz

Figure 3 depicts the PVDF voltage wave number spectrum before and after being controlled for $f=290$ Hz, i.e., near the third structural resonance. The thick lines represent the response of disturbance, while the thin lines denote the response after being controlled. The solid line is obtained on the basis of Eq. (29) which is a continuous function. This figure also contains PVDF voltage wave number spectra derived from the DWT approach for $N=10$, $N=8$, and $N=6$. The acoustic wave number and the Nyquist wave number for different N values are indicated as well. According to this figure, the PVDF voltage wave number spectra obtained from the DWT approach correlate well with those from the CWT approach. If more sensors are applied, i.e., the larger the N implies a closer PVDF voltage wave number spectra derived from the DWT approach to that derived from the CWT approach. Therefore, using an array of PVDF strip films as error sensors, the continuous wave number spectrum can be well approximated. To select either $\Phi_{\kappa,\tilde{v}}$ or $\Phi_{\kappa,\tilde{v}_{DWT}}$ as the cost function, the optimal control voltage input to the PZT actuator can be obtained by LQOCT, respectively. After being controlled, the minimized cost functions are also shown in Fig. 3. This figure indicates that the wavenumber components are globally reduced over the structural wave number. The more sensors used for $\Phi_{\kappa,\tilde{v}_{DWT}}$ implies (a) more reduction of wave number components in the supersonic region, and (b) the closer the remaining wave number spectra to those for $\Phi_{\kappa,\tilde{v}}$.

To further examine the control performance, Fig. 4 depicts the acceleration WTFs before and after being controlled for the PVDF wave number sensing approach. Notably, the sum of the mean square value of the acceleration WTF in the supersonic region is related to the radiated power. The acceleration wave number spectra for either the case $\Phi_{\kappa,\tilde{v}_{DWT}}$ of $N=10$, $N=8$, or $N=6$ after being controlled are close to each other, as well as the approach to that for the case of $\Phi_{\kappa,\tilde{v}}$. The remaining wave number spectra of $|\tilde{A}|^2$ in the supersonic region, which contributes to the far field sound radiations, reveal a combination of the first and second mode response. This finding implies that the most significant radiation mode, i.e., the third mode in this case, is well attenuated and leaves less efficient radiation modes after being controlled. The control mechanism is termed as "modal

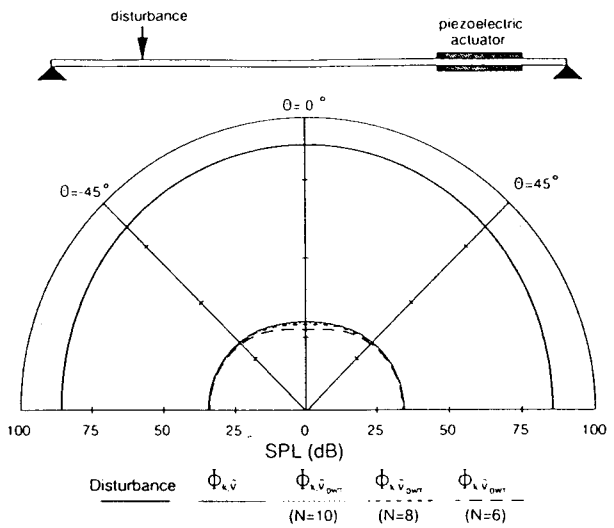

FIG. 5. Sound pressure level distribution for PVDF sensors, $f = 290$ Hz.

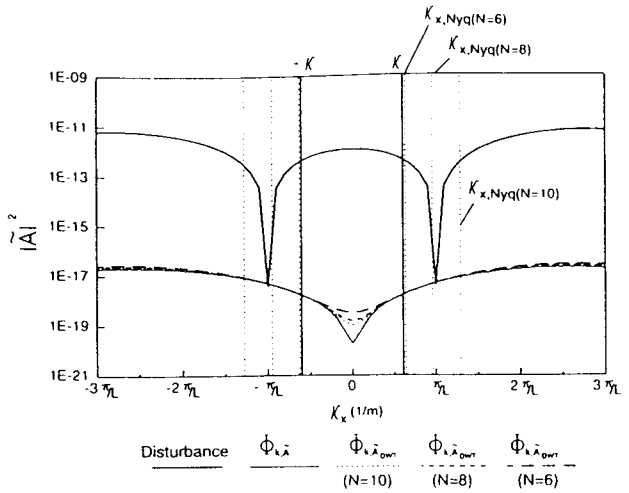

FIG. 7. Acceleration wave number spectra before and after being controlled for accelerometers by CWT approach, $f = 290$ Hz.

suppression."[37] Figure 5 depicts the sound pressure level (SPL) distributions corresponding to the cases in Fig. 4. The SPL distribution due to the disturbance reveals a monopole type radiation pattern. However, the SPL amplitude near $\theta=0°$ is slightly higher than the other amplitudes, thereby confirming the existence of the third mode because the excitation frequency $f = 290$ Hz is near the third structural resonance. The remaining SPL distributions after being controlled reveal an omnidirectional radiation pattern and a small dip near $\theta=0°$. This occurrence can be attributed to that the third mode response is well controlled, leaving less significant radiation modes that are the first and second modes as discussed in Fig. 4.

Above numerical results are based on the use of an array of PVDF strip sensors to implement the wave number sensing approach for beam sound radiation control. Of particular interest is to use an array of accelerometers as error sensors to approximate the wave number transform functions in order to construct the cost functions $\Phi_{\kappa,\tilde{A}_{DWT}}$. Figure 6 presents the acceleration wave number spectra, as derived from

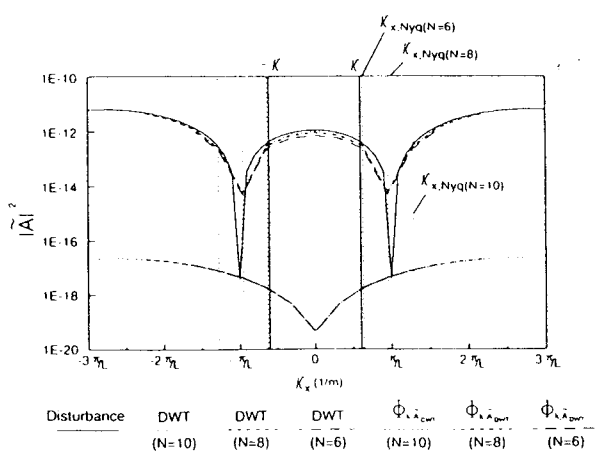

FIG. 6. Acceleration wave number spectra before and after being controlled for accelerometers by DWT approach, $f = 290$ Hz.

the DWT approach before (thin lines) and after (thick lines) being controlled for $N = 10$, $N = 8$, and $N = 6$. The solid line denotes the disturbance. The acoustic wave number and the Nyquist wave number for different N values are also indicated. The acceleration wave number spectra due to the disturbance derived from the DWT approach correlate well with that from the CWT approach. As expected, the more sensors that are applied implies a closer approximation. For selecting $\Phi_{\kappa,\tilde{A}_{DWT}}$ as the cost function to perform wave number sensing approach for controlling sound radiation, according to our results, the acceleration wave number spectra after being controlled derived from the DWT approach are globally reduced. In particular, the value at a point near $\kappa_x = 0$ is relatively small. This small value of κ_x can be referred to as the radiation angle $\phi=0°$, $\theta=0°$. Figure 7 provides the corresponding acceleration wave number spectra derived from the CWT approach after being controlled. The more sensors that are applied imply a smaller wave number component at the dip. If $\Phi_{\kappa,\tilde{A}}$ is selected as the cost function, the acceleration wave number spectrum after being controlled can be seen as a dip at $\kappa_x = 0$, as a dipole response. Figure 8 displays the sound pressure level distributions corresponding to the cases in Fig. 7. The remaining sound pressure level distributions reveal a dipole for the case of $\Phi_{\kappa,\tilde{A}}$, while revealing a small dip near $\theta=0°$ for the cases of $\Phi_{\kappa,\tilde{A}_{DWT}}$. Notably, using more sensors to implement the DWT approach would cause the results to be closer to the CWT approach.

Table I summarizes the reduction of radiated power for both accelerometers and PVDF wave number sensing approach for $f = 290$ Hz. For the case of $\Phi_{\kappa,\tilde{A}}$ which attempts to minimize the acceleration WTF derived from the CWT approach, the reduction of radiated power is the maximum up to 62.5 dB. For the case of $\Phi_{\kappa,\tilde{V}}$ which aims to minimize the PVDF voltage WTF derived from the CWT approach, 57.8 dB is obtained slightly less than that for the case of $\Phi_{\kappa,\tilde{A}}$. For the DWT approach, the accelerometers generally achieve more reduction of radiated power than the PVDF sensors because the accelerometers provide more direct and efficient information regarding radiated sound than the

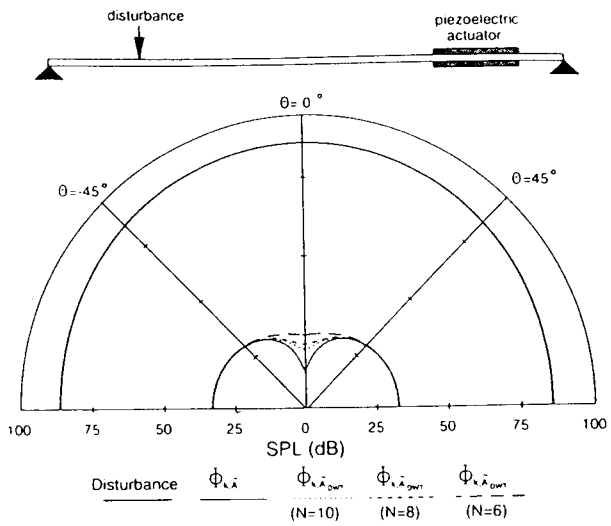

FIG. 8. Sound pressure level distribution for accelerometers, $f = 290$ Hz.

PVDF sensors. For different numbers of sensors applied, the control effectiveness is nearly the same, and more sensors applied for the DWT approach more accurately approximates the results from the CWT approach.

B. Off-resonance excitation case, $f = 350$ Hz

Figure 9 presents the PVDF voltage wave number spectrum before and after being controlled for $f = 350$ Hz, i.e., between the third and fourth structural resonant modes, which is similar to Fig. 3. Again, the PVDF voltage wave number spectra for disturbance from the DWT approach correlate well with those spectra from the CWT approach. More sensors applied can more accurately estimate the wave number spectrum. For using the cost function either $\Phi_{\kappa,\tilde{V}}$ or $\Phi_{\kappa,\tilde{V}_{\mathrm{DWT}}}$, the wave number components in the supersonic region can be markedly reduced; however, spillover may occur in the subsonic region. Corresponding to the cases in Fig. 9, Fig. 10 displays the acceleration wave number spectra before and after being controlled for the PVDF wave number sensing approaches. According to this figure, the wave number components in the supersonic region, which contribute the sound radiation to the far field, are attenuated. In the subsonic region, a spillover can be observed. The control mechanism can be realized in which the supersonic wave number components are well reduced; meanwhile, spillovers

TABLE I. Reduction of the radiated power (dB).

Cost function	$f = 290$ Hz	$f = 350$ Hz
$\Phi_{\kappa,\tilde{V}}$	57.98	9.18
$\Phi_{\kappa,\tilde{V}_{\mathrm{DWT}}}$ $(N = 10)$	58.30	8.92
$\Phi_{\kappa,\tilde{V}_{\mathrm{DWT}}}$ $(N = 8)$	58.53	8.90
$\Phi_{\kappa,\tilde{V}_{\mathrm{DWT}}}$ $(N = 6)$	59.47	7.49
$\Phi_{\kappa,\tilde{A}}$	62.57	16.28
$\Phi_{\kappa,\tilde{A}_{\mathrm{DWT}}}$ $(N = 10)$	62.23	15.94
$\Phi_{\kappa,\tilde{A}_{\mathrm{DWT}}}$ $(N = 8)$	62.01	15.72
$\Phi_{\kappa,\tilde{A}_{\mathrm{DWT}}}$ $(N = 6)$	61.22	14.85

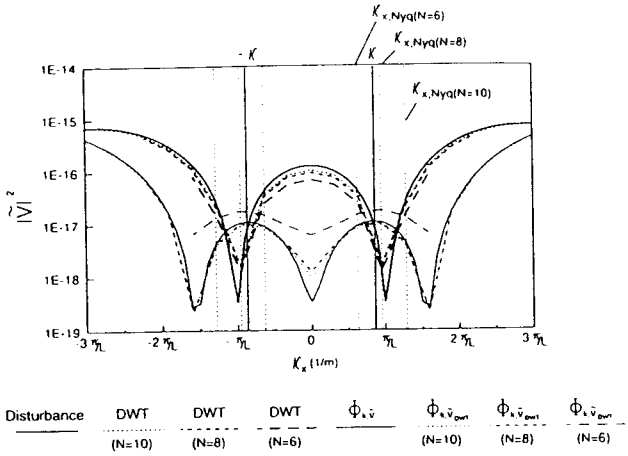

FIG. 9. PVDF voltage wave number spectra before and after being controlled for PVDF sensors, $f = 350$ Hz.

occur for the subsonic wave number components that do not radiate. This control mechanism is called "modal restructuring.[37]" Notably, for the DWT approach $N = 6$, the Nyquist wave number is below the acoustic wave number as shown in Fig. 10. A certain amount of supersonic wave number components can still be reduced because the cost function can be approximately constructed for $N = 6$ as shown in Fig. 9. Figure 11 depicts the sound pressure level distributions corresponding to the cases in Fig. 10.

Examining the performance of using an array of accelerometers for the off-resonance excitation case is of worthwhile interest. Figures 12–14 show the acceleration wave number spectra and sound pressure level distributions, which are similar to Figs. 6–8 except $f = 350$ Hz. Similar characteristics can be observed for off-resonance excitation as those discussed for the PVDF sensors. Table I also indicates that the radiated power reduces for the off-resonance excitation case. The CWT approach is more efficient than the DWT approach. In general, more sensors that are applied for the DWT approach gain more reduction of the radiated power.

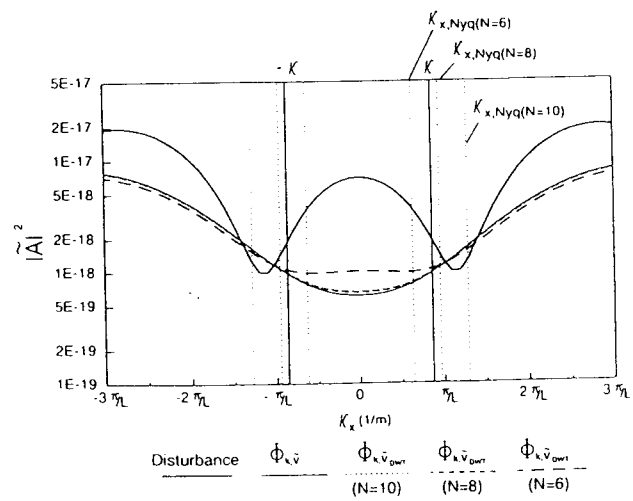

FIG. 10. Acceleration wave number spectra before and after being controlled for PVDF sensors, $f = 350$ Hz.

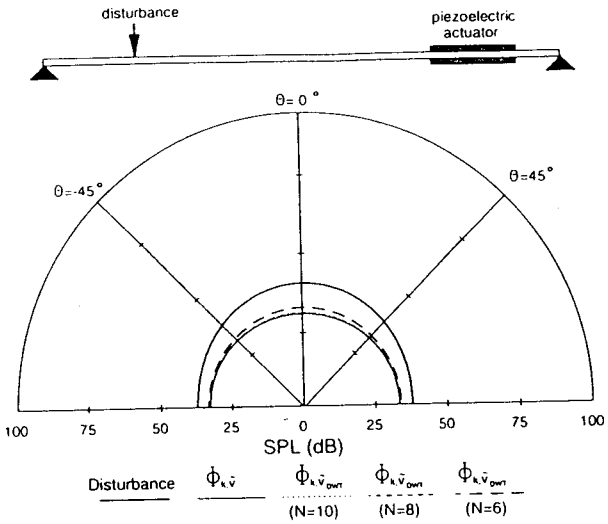

FIG. 11. Sound pressure level distribution for PVDF sensors, $f=350$ Hz.

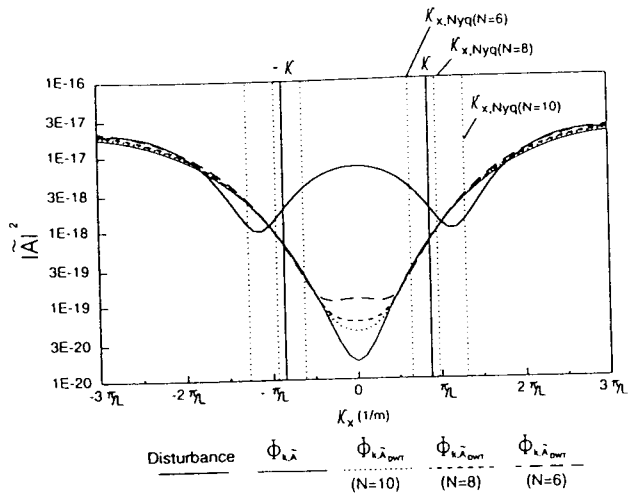

FIG. 13. Acceleration wave number spectra before and after being controlled for accelerometers by CWT approach, $f=350$Hz.

C. Different excitation frequency performance

As mentioned earlier, only the wave number components below or above the positive or negative Nyquist wave number are valid for discrete wave number transform. If wave number components in supersonic region lie above the Nyquist wave number, increasing the number of sensors is inherently required. Another alternative involves properly designing the PVDF sensor to suppress the higher wave numbers so that the effect of subsonic wave numbers will not be eliminated.[15,30] Further investigating in the shape design of PVDF sensor for the wave number sensing approach would be a worthwhile pursuit. Table II lists the minimum number of sensors for different excitation frequencies. For $f=300$ Hz, the acoustic wave number is 5.495, and the minimum N_κ is then 4 in order to include all of the supersonic wave number components; therefore, the minimum number of sensors N is 6, and its corresponding Nyquist wave number is 7.894. If $N=10$, then the Nyquist wave number is 13.15. Sound radiation control can be effective up to $f=700$ Hz, i.e., the corresponding acoustic wave number is 12.82.

Moreover, the performance of the PVDF and accelerometers wave number sensing approaches is further evaluated for different excitation frequencies. Figure 15(a)–(d), respectively, plots the cost functions against excitation frequency before and after being controlled for the cases of $\Phi_{\kappa,\tilde{A}}$, $\Phi_{\kappa,\tilde{V}}$, $\Phi_{\kappa,\tilde{A}_{DWT}}$, and $\Phi_{\kappa,\tilde{V}_{DWT}}$. As those figures reveal, the cost functions can be attenuated significantly after being controlled. This finding suggests that the minimization process effectively reduces the cost functions while applying controls. The effectiveness of sound radiation control can be studied by examining the radiated power versus excitation frequency, as shown in Fig. 16. Several observations are summarized as follows:

(1) For accelerometers by the CWT approach, i.e., the cost

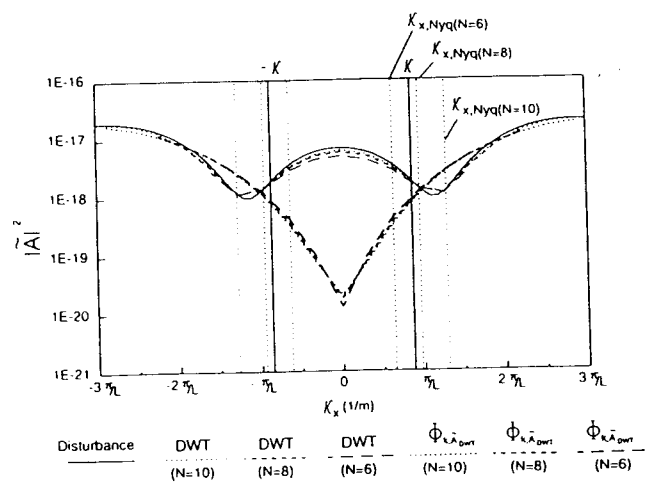

FIG. 12. Acceleration wave number spectra before and after being controlled for accelerometers by DWT approach, $f=350$ Hz.

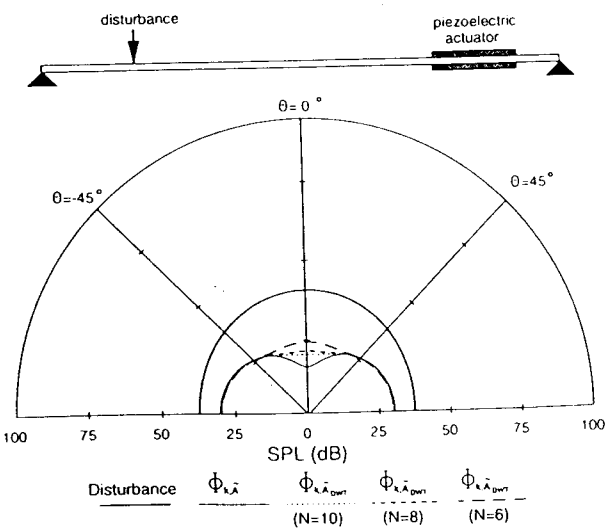

FIG. 14. Sound pressure level distribution for accelerometers, $f=350$ Hz.

TABLE II. Minimum number of sensors for different excitation frequencies. Note $\Delta\kappa_x = 1/L = 2.6315$ 1/m. $\kappa_{x,\mathrm{Nyq}} = (N/2)\Delta\kappa_x$.

f (Hz)	100	200	300	400	500	600	700	800
$\kappa = 2\pi f/c$	1.831	3.663	5.495	7.327	9.159	10.99	12.82	14.65
N_κ	2	3	4	4	5	6	6	7
$(N_\kappa - 1)\Delta\kappa_x$	2.631	5.263	7.894	7.894	10.52	13.15	13.15	15.78
min(N)	2	4	6	6	8	10	10	12
$\kappa_{x,\mathrm{Nyq}}$	2.631	5.263	7.894	7.894	10.52	13.15	13.15	15.78

function $\Phi_{\kappa,\tilde{A}}$ is chosen, the reduction of the radiated power is most effective throughout the frequency range. However, it cannot be implemented in practice.

(2) For either the CWT or DWT approach, the accelerometers based wave number sensing approach generally controls sound radiation more effectively than the PVDF sensors because the defined cost function for the accelerometers is more directly related to the radiated power than that for the PVDF sensors.

(3) For both accelerometer and PVDF based wave number sensing approaches, the DWT approach can achieve approximately the same control effectiveness as the CWT approach. The DWT approach can be practically implemented by using an array of evenly spaced accelerometers[28,29] or PVDF strip sensors.

(4) With the use of the PVDF sensors for wave number sensing approach, the control is ineffective for some off-resonance excitation cases. The optimal location of the control PZT actuator can be a critical factor. The optimal location of the PZT actuator, in conjunction with the use of the PVDF wave number sensing technique, is under investigation.

III. CONCLUSIONS

This study presents a novel wave number sensing approach which uses an array of PVDF strip sensors. By per-

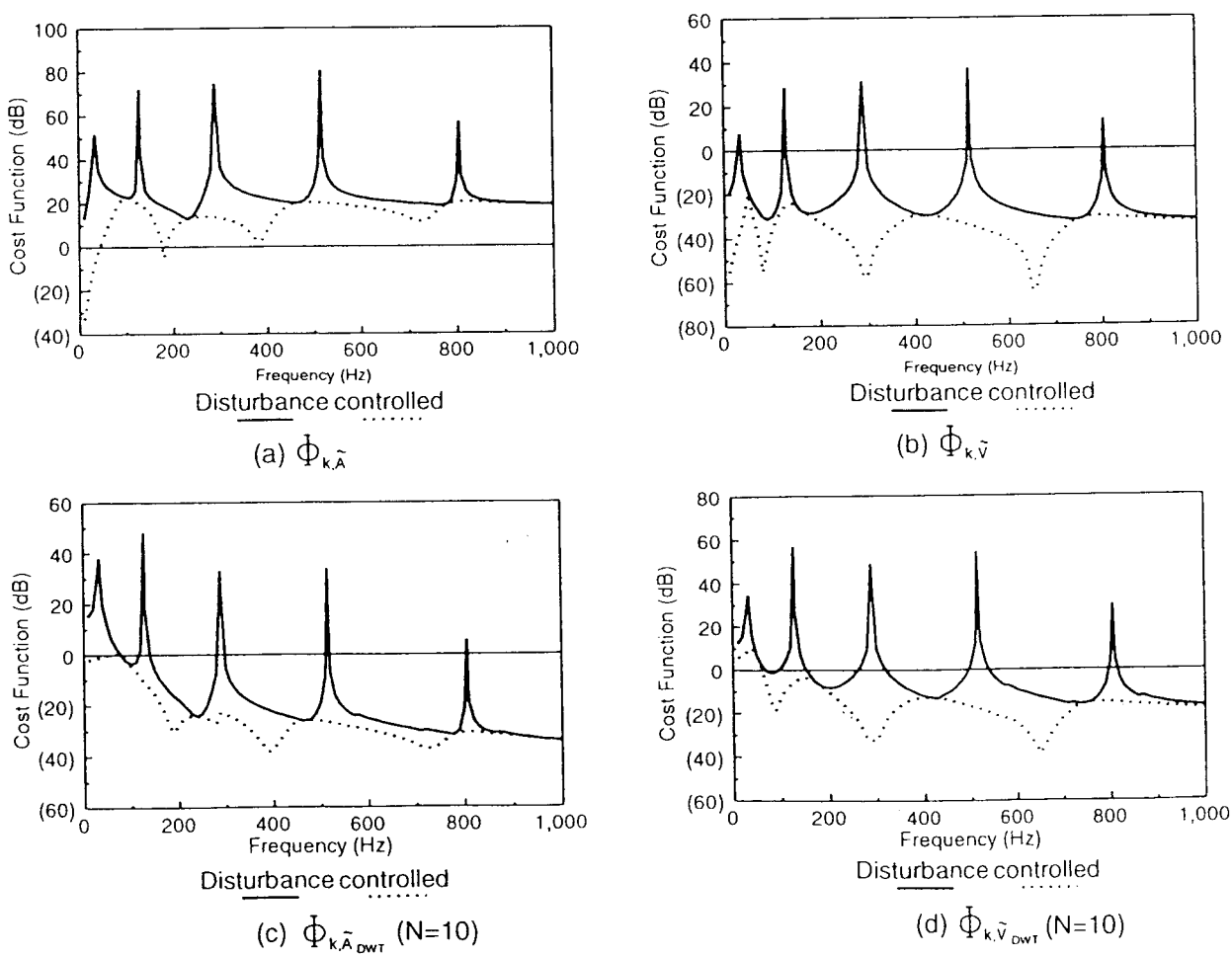

FIG. 15. Cost functions versus excitation frequency.

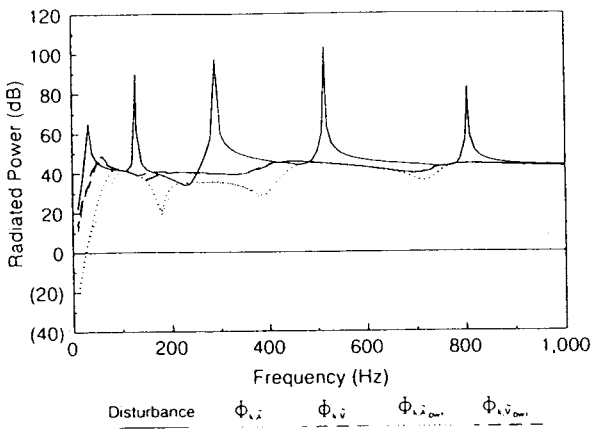

FIG. 16. Radiated power versus excitation frequency.

forming the discrete wave number transform on the sensor signals allows us to obtain the wave number transform functions. The cost function can then be defined as the sum of mean square values of PVDF voltage wave number transform functions in the supersonic region. The PVDF based wave number sensing approach, in conjunction with the use of the LMS feedforward control algorithm, is also applied to control the sound radiation of a baffled simply supported beam. The beam is assumed to be subjected to a harmonic point force disturbance; meanwhile, the PZT patches are applied as control actuators. Analysis results demonstrate that the PVDF based wave number sensing approach can aptly control sound radiation. Sound pressure level distribution and wave number analysis is also performed to examine the control mechanism. The accelerometers as error sensors for the wave number sensing approach, are also considered. Both continuous and discrete wave number transform approaches are compared as well. According to that comparison, the wave number transform function derived from the CWT approach can be well approximated by the DWT approach, thereby allowing the wave number transform functions to be practically measured by either an array of accelerometers or PVDF sensors. The accelerometers generally perform better sound radiation control than the PVDF sensors. In particular, for some off-resonance frequency excitation, the PVDF wave number sensing approach may not be efficient. To improve the control effectiveness for the off-resonance excitation, the optimal placement of the control actuator can be a feasible solution. This work not only enhances the sensing abilities of intelligent materials structure systems, but also provides a valuable reference for further efforts to control structural sound radiation control.

ACKNOWLEDGMENTS

The author would like to thank the National Science Council, Republic of China, for financially supporting this work under Contract No. NSC84-2212-E-020-005. The reviewers are also appreciated for their valuable comments and suggestions, particularly with the formulations of the negative wave numbers.

[1] J. Jones and C. R. Fuller, "Active control of sound fields in elastic cylinders by multiple forces," AIAA J. **27**, 845–852 (1989).
[2] E. K. Dimitriadis, C. R. Fuller, and C. A. Rogers, "Piezoelectric actuators for distributed vibration excitation of thin plates," J. Vib. Acoust. **113**, 100–107 (1991).
[3] B. T. Wang, E. K. Dimitriadis, and C. R. Fuller, "Active control of structurally radiated noise using multiple piezoelectric actuators," AIAA J. **29**, 1802–1809 (1991).
[4] C. Liang, C. A. Rogers, and C. R. Fuller, "Acoustic transmission and radiation analysis of adaptive shape memory alloy reinforced laminated plates," J. Sound Vib. **144**, 475–482 (1991).
[5] R. L. Clark and C. R. Fuller, "Control of sound radiation with adaptive structures," J. Intell. Mater. Syst. Struct. **2**, 431–452 (1992).
[6] L. Meirovitch and S. Thangjitham, "Active control of sound radiation pressure," J. Vib. Acoust. **112**, 237–244 (1990).
[7] B. T. Wang, "Active control of far-field sound radiated by a beam with piezoelectric control transducers: Physical system analysis," Smart Mater. Struct. **3**, 476–484 (1994).
[8] S. J. Elliott, I. M. Stothers, and P. A. Nelson, "A multiple error LMS algorithm and its application to the active control of sound and vibration," IEEE Trans. Acoust., Speech, Signal Process. **35**, 1423–1434 (1987).
[9] R. A. Burdisso and C. R. Fuller, "Theory of feedforward controlled system eigenproperties," J. Sound Vib. **153**, 437–451 (1992).
[10] W. T. Baumann, W. R. Saunders, and H. H. Robertshaw, "Active suppression of acoustic radiation from impulsively excited structures," J. Acoust. Soc. Am. **90**, 3202–3208 (1991).
[11] C. Deffayet and P. A. Nelson, "Active control of low frequency harmonic sound radiated by a finite panel," J. Acoust. Soc. Am. **84**, 2192–2199 (1988).
[12] H. C. Lester and C. R. Fuller, "Active control of propeller induced noise fields inside a flexible cylinder," AIAA J. **28**, 1374–1380 (1990).
[13] C. K. Lee and F. C. Moon, "Modal sensors/actuator," J. Appl. Mech. **57**, 434–441 (1990).
[14] J. E. Hubbard, Jr., "Distributed sensors and actuator for vibration control in elastic components," Noise-Con 87, 407–412 (1987).
[15] R. L. Clark, C. R. Fuller, and R. A. Burdisso, "Design approaches for shaping polyvinylidene fluoride sensors in active structural acoustic control," J. Intell. Mater. Syst. Struct. **4**, 354–365 (1993).
[16] C. R. Fuller and J. D. Jones, "Influence of sensor and actuator location on the performance of active control systems," 87-WA/NCA-9, ASME Annual Meeting, Boston, MA (1987).
[17] B. T. Wang and C. R. Fuller, "Evaluation of different forms of cost functions in the design of active structural-acoustic control systems," Noise-Con 87 (1991).
[18] B. T. Wang, "The performance of accelerometers, microphones and PVDF sensors in active structural acoustic control: Theoretical analysis," Chin. J. Mech. **10**, 205–212 (1993).
[19] R. L. Clark and C. R. Fuller, "Modal sensing of efficient acoustic radiators with polyvinylidene fluoride distributed sensors in active structural acoustic control approaches," J. Acoust. Soc. Am. **91**, 3321–3329 (1992).
[20] R. L. Clark and C. R. Fuller, "Optimal placement of piezoelectric actuators and polyvinylidene fluoride error sensors in active structural acoustic control approaches," J. Acoust. Soc. Am. **92**, 1521–1533 (1992).
[21] Y. Gu, R. L. Clark, C. R. Fuller, and A. C. Zander, "Experiments on active control of plate vibration using piezoelectric actuators and polyvinylidene fluoride (PVDF) modal sensors," J. Vib. Acoust. **116**, 303–308 (1994).
[22] S. D. Snyder, C. H. Hansen, and N. Tanaka, "Shaped vibration sensors for feedforward control of structural radiation," Proceedings of the Second Conference on the Recent Advances in Active Control of Sound and Vibration, 177–188 (1993).
[23] F. Charette, C. Guigou, and A. Berry, "Development of volume velocity sensors for plates using PVDF film," Proceedings of ACTIVE 95, 241–252 (1995).
[24] F. Fahy, *Sound and Structural Vibration: Radiation, Transmission, and Response* (Academic, Orlando, FL, 1985), pp. 72–81.
[25] B. T. Wang and C. R. Fuller, "Near-field pressure, intensity, and wave number distributions for active structural acoustic control of plate radiation: Theoretical analysis," J. Acoust. Soc. Am. **92**, 1489–1498 (1992).
[26] C. R. Fuller and R. A. Burdisso, "A wave number domain approach to the active control of structure-borne sound," J. Sound Vib. **148**, 335–360 (1991).
[27] R. L. Clark and C. R. Fuller, "A model reference approach for imple-

menting active structural acoustic control," J. Acoust. Soc. Am. **92**, 1534–1544 (1992).
[28] J. P. Maillard and C. R. Fuller, "Advanced time domain wave-number sensing for structural acoustic systems. I. Theory and design," J. Acoust. Soc. Am. **95**, 3252–3261 (1994).
[29] J. P. Maillard and C. R. Fuller, "Advanced time domain wave-number sensing for structural acoustic systems. II. Active radiation control of a simply supported beam," J. Acoust. Soc. Am. **95**, 3261–3272 (1994).
[30] B. L. Scott and S. D. Sommerfeldt, "Estimating acoustic radiation from a Bernoulli–Euler beam using shaped polyvinylidene flouride film," J. Acoust. Soc. Am. **101**, 3475–3485 (1997).
[31] L. Cremer and M. Heckl, *Structure-Borne Sound: Structural Vibrations and Sound Radiation at Audio Frequencies* (Springer-Verlag, Berlin, 1988), pp. 528–529.
[32] B. T. Wang, "Characterization of transfer functions for piezoceramic and conventional transducers," J. Intell. Mater. Syst. Struct. **7**, 390–398 (1996).
[33] B. T. Wang, "Feasibility analysis of using piezoceramic transducers for cantilever beam modal testing," Smart Mater. Struct. **6**, 106–116 (1997).
[34] B. T. Wang, *Active Structural Acoustic Control of Intelligent Material Structure System* (NSC Report No. NSC82-0410-E-020-001, Taiwan, R.O.C., 1993), pp. 16–23.
[35] Piezo Systems, Inc., *Product Catalog* (Cambridge, MA, 1990).
[36] Pennwalt Corporation, *Piezo Film Sensor Application Notes* (Valley Forge, PA, 1990).
[37] C. R. Fuller, C. H. Hansen, and S. D. Snyder, "Active control of sound radiation from a vibrating rectangular panel by sound sources and vibration inputs: An experimental comparison," J. Sound Vib. **145**, 195–215 (1991).